Steam Oxidation of 80Ni-20Cr High-Velocity Oxyfuel Coatings on 9Cr-1Mo Steel: Diffusion-Induced Phase Transformations in the Substrate Adjacent to the Coating

T. SUNDARARAJAN, S. KURODA, and F. ABE

The steam oxidation resistance of 80Ni-20Cr coatings on modified 9Cr-1Mo steel has been evaluated in the temperature range of 600 °C to 750 °C. High-velocity oxyfuel (HVOF) spray was used for the coating process. The steam-oxidized specimens exhibited the diffusion of iron from the substrate to the coating and diffusion of nickel from the coating to the substrate. Nickel diffusion to the substrate adjacent to the coating induced the microstructural changes. Micro X-ray diffraction (XRD) studies and energy-dispersive spectroscopy (EDS) point analysis on these transformed zones revealed that the newly formed phases are the austenite in the high-Ni-concentration region and the martensite in the low-Ni-concentration region. Microhardness studies showed higher hardness values in the martensite zones.

I. INTRODUCTION

INCREASING the steam temperature for the boiler and the turbine components of a power plant, which enhances the thermal efficiency, has necessitated the development of advanced ferritic heat-resistant steels with sufficient creep-rupture strength and steam-oxidation resistance at high temperatures. Tempered martensite with 9 to 12 wt pct Cr strengthened with minor alloying elements has attracted much interest for application in high-temperature plants, such as coal-fired ultrasupercritical (USC) power plants at temperatures higher than 600 °C.[1] The improvement of creep strength has been reported for the 9Cr steel by optimizing the minor alloying elements, such as W, Mo, and B, to obtain a desirable precipitation and solid-solution strengthening.[2,3,4] However, the steam-oxidation resistance of such alloys is not satisfactory. The addition of 3 pct Pd to the 9 pct Cr–based steel remarkably improved the oxidation resistance, but the cost of Pd is restricting its use in actual plants.[5]

In the recent past, thermal-spray technology has been extensively used in high-temperature applications such as aerospace and power generation.[6,7,8] The thermal-spray process has the potential to overcome the steam oxidation of USC boiler components, since it can offer a thick film and flexibility to deal with on-site modifications.[9–15] In our earlier studies, HVOF coatings of 80Ni-20Cr and 50Ni-50Cr on modified 9Cr-1Mo steel showed the excellent steam-oxidation resistance in the tested duration of 1000 hours. The formation of chromium oxide on the top surface of the coating protected the material against steam oxidation.[9–12]

The coating adhesion to the substrate is of crucial importance for the present application; otherwise, the scale growth will be accelerated in the areas of delaminated coating due to an anomalous temperature rise. A delaminated scale or coating can damage the turbine in the down-stream as well. The factors affecting the adhesive strength of the coatings are mainly (1) the generation of the residual stress, (2) thermal shock, and (3) diffusion behavior. In our earlier studies, we have reported the excellent adhesive strength of 80Ni-20Cr coatings after aging and thermal-cycling tests.[14,15] The aged and thermal-cycled specimens showed increased adhesive strength compared to the as-coated condition. The increased adhesive strength of the 80Ni-20Cr coatings on the modified 9Cr-1Mo steel was attributed to the diffusion of Ni from the coating to the substrate and the diffusion of Fe from the substrate to the coating. On the contrary, diffusion across the 50Ni-50Cr coating/substrate interface was essentially blocked by the formation of a continuous chromium carbide layer along the interface, which led to a moderate reduction in the adhesive strength of the coating.[14,15] The Ni-Cr coatings showed a similar diffusion phenomenon when they were exposed to either air or the steam.

Diffusion between a coating and the underlying substrate is a common phenomenon when the coating is exposed to high temperatures. Even if the coating evinced a higher adhesive strength due to the diffusion process, it can cause several other problems in the extended period of aging. For example, in the case of thermal-barrier coatings, a NiCrAlY bond coat is usually placed over the Ni-based superalloy substrate. The oxidation resistance of the coating arises from the Al present in the coating forming the α-aluminum oxide. However, the Al tends to diffuse into the Ni-based substrate alloy and forms the porous Ni_3Al, which affects both the oxidation resistance of the coating and the mechanical properties of the substrate.[16] The aforementioned phenomenon suggests the importance of revealing the change in the phase and the microstructure resulting from the diffusion process. Additionally, the continuous diffusion of Ni from the 80Ni-20Cr coating to the substrate would lead to the Ni deficiency in the coating, which would result in the damage of the coating's compositional integrity and, subsequently, its steam-oxidation resistance. In the present investigation, an attempt was made to understand the diffusion-induced changes after the steam oxidation. The kinetics of this diffusion process as a function of temperature as well as test duration has also been studied.

T. SUNDARARAJAN, Researcher, Steel Research Center, S. KURODA, Director, Thermal Spray Group, and F. ABE, Heat Resistance Design Group, are with the National Institute for Materials Science, Tsukuba, 305-0047, Japan. Contact e-mail: rajan.sundar@nims.go.jp

Manuscript submitted August 5, 2004.

Table I. Chemical Composition of the Substrate and Coating Powder (Mass Percent)

Material	C	P	S	Si	Mn	Cr	Ni	Mo	Cu	V	Al	N	Nb	Fe
9Cr-1Mo	0.10	0.005	0.001	0.24	0.44	8.74	0.04	0.94	0.01	0.21	0.04	0.058	0.076	bal
80Ni-20Cr	0.03	0.005	0.025	0.90	0.92	19.7	bal	—	—	—	—	—	—	0.82

II. EXPERIMENTAL

A 9Cr-1Mo–type ferritic steel was used as the substrate specimen. Specimens with dimensions of 10 mm (length) × 10 mm (width) × 4 mm (thickness) were coated with 80Ni-20Cr powder (manufactured by Praxair) by thermal spraying. The chemical composition of the substrate and the powder are presented in Table I. The substrate was heat treated as specified by the NRIM creep data sheet to obtain the tempered martensite microstructure.[17] The specimens were sand blasted using alumina powder for better adhesion of the sprayed coatings before spraying. Thermal-spray coatings were deposited using a HVOF spray process (JP 5000, TAFA, Praxair). Six passes were adopted, including the two passes for preheating the substrate. The process parameters used for HVOF coating are listed in Table II. The thickness of the coating obtained was about 60 μm. The coated specimens were subjected to X-ray diffraction (XRD) and scanning electron microscope (SEM) investigations before placing them into the steam-oxidation chambers.

Steam-oxidation tests were carried out at different temperatures, viz., 600 °C, 650 °C, 700 °C, and 750 °C. Figure 1 schematically represents the steam-oxidation test procedure carried out in the present study. The test chambers were filled with Ar gas and then evacuated using a rotary pump. This process was repeated 3 times to remove the residual air present in the chamber. Subsequently, the chambers were heated to the desired test temperatures in 3 hours. When the chamber temperature exceeded 200 °C, steam was introduced into the chambers under a pressure of 1.67×10^3 m^3/s. A steam flow of 0.03 m/s was maintained inside the furnace during the experiments. The water used to produce the steam contained less than 10 ppb of oxygen, and the conductivity was kept below 0.08 μS. After the completion of the test duration, the chamber temperature was brought to 200 °C in 12 hours and steam purging was stopped at the end of this process. Another 24 hours was allowed to cool the chamber before the specimens were taken out. The sample pieces were taken out at different durations, namely, after 10, 100, and 1000 hours of steam oxidation. Each time the samples were taken out, the chamber was brought to room temperature and the entire aforementioned procedure was repeated for further testing durations. This might have helped to simulate the thermal cycling which occurs in real plant operation, where shut-downs would happen depending on the power requirement and maintenance. The surfaces of oxidized specimens were analyzed by XRD to identify new phases formed during steam oxidation. The SEM and electron-probe microanalysis (EPMA) studies were carried out on the cross sections to reveal the change in microstructure and composition of the coating and the underlying substrate after the steam oxidation.

For the microstructural examinations, the polished specimen cross section was etched with vilellas reagent (100 mL ethyl alcohol + 5 mL HCl + 4 g picric acid) for 20 seconds.

Table II. Spray Parameters Used for HVOF Spray Process

Fuel flow rate	0.379 L/min
Oxygen flow	861 sL/min
Barrel length	102 mm
Torch traverse speed	700 mm/s
Spray distance	380 mm
Powder feed gas	nitrogen
Powder size	22 to 53 μm

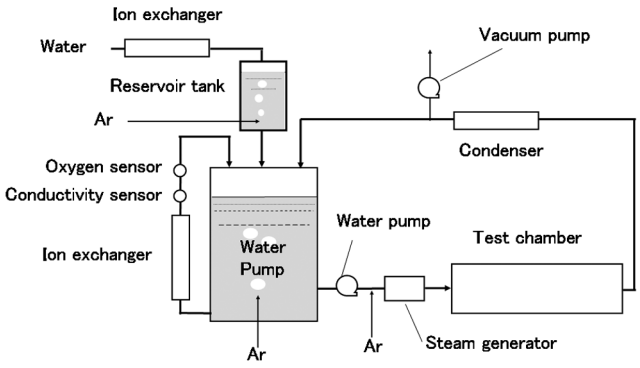

Fig. 1—Schematic representation of the steam-oxidation test apparatus.

Subsequently, the specimens were cleaned with the deionized water and dried before examining them with the SEM. Microhardness studies were carried out on the cross sections of the steam-oxidized specimens in comparison to the as-coated conditions. The load applied for each indentation was 50 g.

Micro XRD studies were carried out on the cross section of the steam-oxidized samples. The incident X-rays were allowed to pass through a 10 μm pinhole aperture and to fall on a specific portion of the substrate. The points to be analyzed were identified with a close-coupled device camera attached to the XRD system. In order to explain the phase changes in the steel substrate adjacent to the coating, the Thermo-Calc software package was used to calculate the stable phases of the steel with the addition of Ni over the wide temperature range.

III. RESULTS

A. *Coating Structure and Morphology*

Figure 2 shows the backscattered electron (BSE) image cross sections for the as-coated and steam-oxidized (750 °C/1000 hours) specimens. The as-coated specimen shows a dense and uniform coating with a thickness of about 60 to 70 μm. All the 80Ni-20Cr coatings exhibited neither delamination from the substrate nor scale initiation at the coating/surface interface after 1000 hours of steam-oxidation tests. This confirms the excellent steam-oxidation resistance of 80Ni-20Cr coatings on modified 9Cr-1Mo steel.

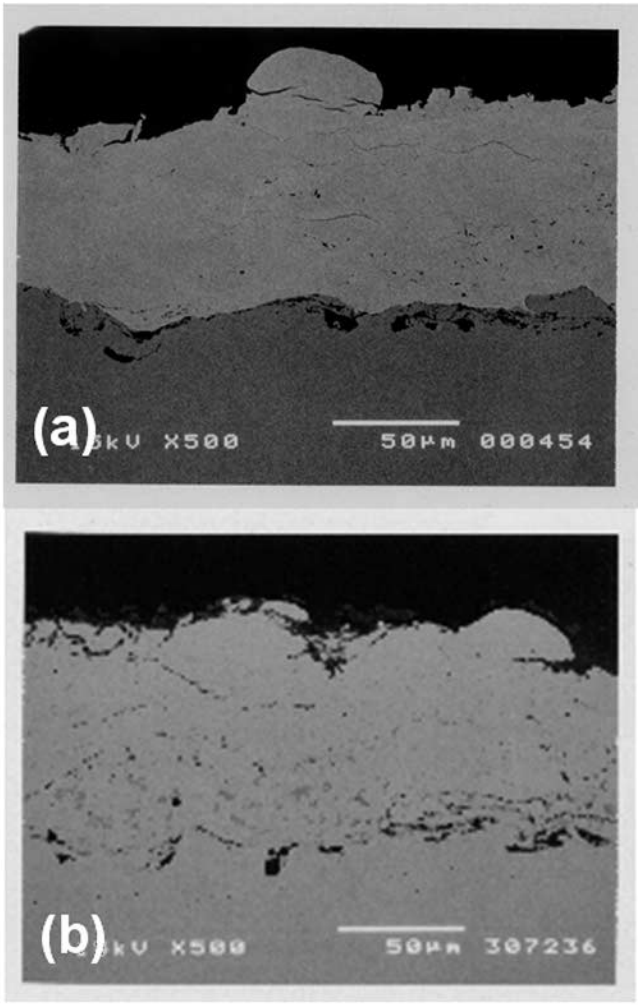

Fig. 2—BSE image cross sections of the 80Ni-20Cr-coated modified 9Cr-1Mo steel specimens: (*a*) as-coated and (*b*) steam oxidized at 750 °C for 1000 h.

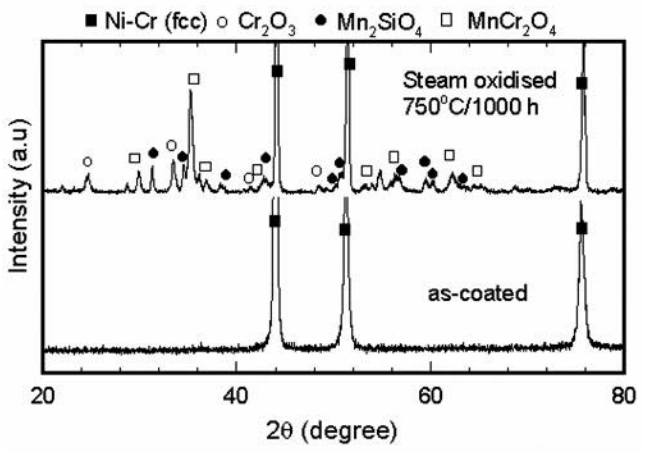

Fig. 3—XRD spectra of the 80Ni-20Cr coating on 9Cr-1Mo steel: as-coated and steam oxidized at 750 °C for 1000 h.

Figure 3 shows the XRD pattern for the as-coated and steam-oxidized (750 °C/1000 hours) 80Ni-20Cr coatings. The three prominent peaks seen for the as-coated specimen

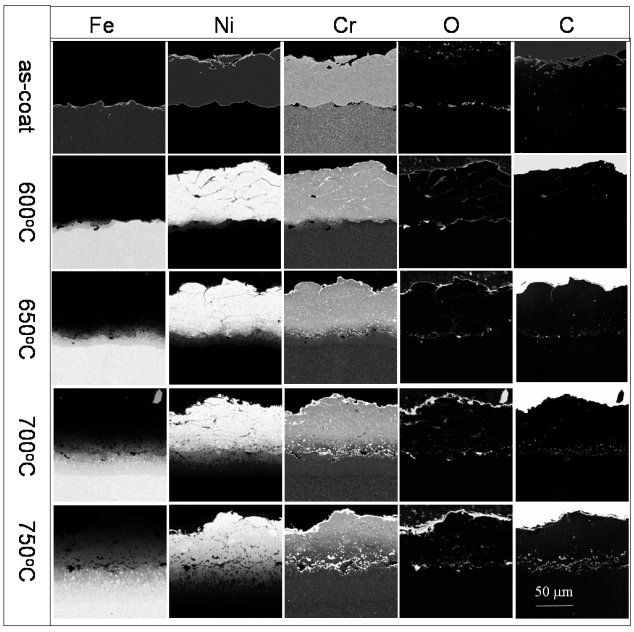

Fig. 4—EPMA elemental mapping of the 80Ni-20Cr coatings steam oxidized at different temperatures for 1000 h, in comparison with the as-coated condition.

are indexed to the Ni-Cr fcc phase. No oxide phase could be detected from the XRD pattern. After steam oxidation at 750 °C for 1000 hours, the XRD pattern shows several minor peaks along with the major Ni-Cr fcc peaks. The minor peaks are indexed to three different oxides/spinels, such as Cr_2O_3, $MnCr_2O_4$, and Mn_2SiO_4. It should be noted that the elements such as Mn and Si in the feed stock powder for the coating are below 1 mass pct (Table I). During steam oxidation, however, Mn and Si segregated to the top surface and formed the spinel.[8] However, the XRD pattern does not show any peaks corresponding to oxides of Fe, suggesting that there was no scale growth originating from the substrate.

B. *The EPMA Studies*

Figure 4 shows the EPMA elemental mapping for the 80Ni-20Cr coatings on the modified 9Cr-1Mo steel substrate steam oxidized for 1000 hours at four different temperatures, as compared with the as-coated condition. In the as-coated condition, Fe is present in the substrate region and Ni is present in the coating region, exhibiting a sharp concentration boundary at the coating/substrate interface. Elemental mapping for Cr shows that it is present both in the coating and the substrate regions. The Cr intensity within the coating is higher than in the substrate, because the coating possesses a higher Cr concentration (20 wt pct) than the substrate (9 wt pct) (Table I). The oxygen mapping for the as-coated conditions does not show any intense lines within the coating region. Several bright dots at the coating/substrate interface are due to residual alumina particles used for the blast cleaning of the substrate. The elemental mapping for the steam-oxidized samples of every element shows significant changes. The specimen steam oxidized at 600 °C for 1000 hours shows a small amount of Ni diffusion from the coating to the substrate. Similarly, Fe diffused from the substrate to the coating. Although Cr did not undergo much interdiffusion, it

shows an enrichment at the surface of the coating. Oxygen mapping for the respective specimen also exhibits an enrichment at the surface, indicating that on steam oxidation, Cr-rich oxide was formed at the surface of the coating. With an increase of temperature from 600 °C to 650 °C, the diffusion of Ni from the coating to the substrate and the diffusion of Fe from the substrate to the coating increased. In the case of the specimen steam oxidized at 750 °C, the diffusion front at either side reached a distance of more than 50 μm. This indicates that the diffusion of Ni and Fe increased with an increase in temperature. In the case of Cr and O mapping, both the elements show further enrichment at the surface for all the tested conditions.

Unlike Ni, Cr did not diffuse into the substrate, which is evident from the Cr map in the substrate zone, where the Cr concentration is almost uniform. It was reported that both Ni and Cr diffuse almost at the same rate (the diffusion coefficient for Cr is 1.79×10^{-9} and that for Ni is 6.4×10^{-10} m^2/s at 750 °C) into the Fe-based systems.[18,19] However, in the present study, Cr did not diffuse into the substrate because of the chromium carbide formation. Since C diffuses much faster than Cr, chromium carbide precipitated in the lower region within the coating. In our earlier studies,[10] steam oxidation of 50Ni-50Cr coatings on a modified 9Cr-1Mo steel substrate yielded a continuous chromium carbide layer at the coating/surface interface. The formation of the carbide at the interface acted as a barrier for the Ni and Fe diffusions. The 80Ni-20Cr coating did not yield a continuous chromium carbide layer, which allowed the diffusion of Fe and Ni across the coating/substrate interface.

Figure 5 shows the distance of the Ni and Fe diffusion fronts from the coating/substrate interface with test duration at 750 °C. In the specimens steam oxidized for 10 hours, Fe and Ni showed nearly 8 μm outward and inward diffusions, respectively, which extended to about 23 μm after 100 hours and to about 64 μm after 1000 hours.

Under the condition of an instantaneous thin-film source of the diffusing species into a semi-infinite solid, the diffusion profile that follows from Fick's second law is, therefore, typically linear in plots of ln *c vs* penetration distance squared. The diffusion distance (x) can be defined as

$$x^2 \propto t \qquad [1]$$

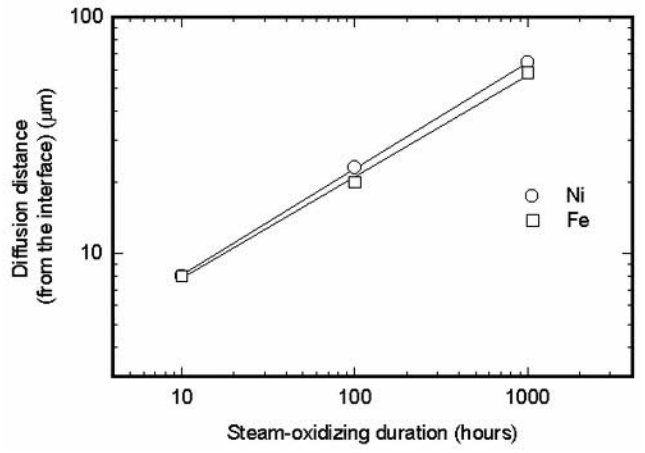

Fig. 5—Diffusion distance of Fe and Ni as a function of time during steam oxidation at 750 °C.

From Eq. [1], the plot of log x *vs* log t should give the slope value of 0.5. From Figure 4, the slope values for Ni and Fe are found to be 0.45 and 0.43, respectively, suggesting that the diffusion closely approaches the linear diffusion process. Although the diffusion of both Ni and Fe had almost a similar diffusion rate at 750 °C, there are several other factors that have to be considered for this diffusion process. The Ni-Cr coating consist of a large number of vacancies, which might facilitate the faster diffusion Fe atoms.

C. *Microhardness Studies*

Continuous diffusion of Ni into the substrate during steam oxidation is expected to cause changes in the microstructure and the mechanical properties of the substrate region adjacent to the coating. Microhardness studies were carried out on the cross sections of the steam-oxidized as well as as-coated specimens across the coating/substrate interface. Figure 6(a) shows the microhardness distribution of the as-coated specimen. The optical micrograph embedded in the plot indicates the actual measurement points. In the coating region, all measured points showed similar values around 400 Hv. In the substrate region, a slightly higher value of hardness was obtained close to the coating/substrate interface than the at the core substrate. The reason for the increased hardness in the substrate near the coating/substrate interface was attributed to the work hardening produced by the sandblasting of the substrate prior to the coating process as well as by the impingement of HVOF-sprayed particles. The core substrate showed the hardness value of 240 Hv, which is normally expected for such a modified 9Cr-1Mo steel with a tempered martensite microstructure.

Figure 6(b) shows the microhardness values obtained for the particular specimen steam oxidized at 750 °C for 1000 hours. In the coating portion, the hardness was reduced to around 250 Hv after steam oxidation. It is well known for such HVOF metallic coatings that the as-coated specimen contains a high amount of dislocations due to the peening effects of the high-velocity particles, which enhances the hardness value of the coating. During steam oxidation, the high temperature acted as an annealing process. In the substrate region, the optical micrograph shows some changes in the microstructure near the interface region. The region near the interface has a microhardness value of 235 Hv. Further down, toward the core substrate, the microhardness reaches its highest value of 340 Hv. The core substrate region of the steam-oxidized specimen has a microhardness value of 218 Hv. It is likely that the higher values observed in

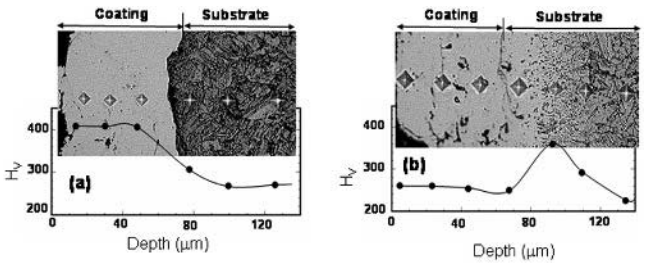

Fig. 6—Distribution of microhardness for the (*a*) as-coated specimen and (*b*) steam-oxidized 80Ni-20Cr coating sprayed on a modified 9Cr-1Mo steel.

the substrate region arise from the diffusion of Ni from the coating to the substrate during steam oxidation.

Figure 7(a) shows the effects of temperature on the microhardness variations across the coating and the substrate adjacent to the coating after 1000 hours. In the coating region, the hardness of the steam-oxidized specimens decreased compared to the as-coated condition. However, the values obtained across the coating for each specimen were almost constant. The EPMA elemental mapping shows that with an increase of temperature, the diffusion of Fe also increased to produce a significant concentration gradient. Nevertheless, the Fe diffusion had the least influence on the coating hardness. However, the substrate zone shows remarkable differences in the microhardness distribution for each tested condition. The specimen steam oxidized at 600 °C shows lower hardness values at the near-interface region compared to the core substrate and does not show any localized increase in the hardness values, unlike the specimen steam oxidized at 750 °C (Figure 5(b)). The specimen steam oxidized at 650 °C shows a small increase in hardness value near the interface, whereas at 700 °C and 750 °C, the samples show increased hardness at this region (adjacent to the coating). All the results suggest that the steam-oxidized specimens produced a hard layer in the substrate adjacent to the coating, except for the sample tested at the temperature of 600 °C.

Figure 7(b) shows the effects of test duration on the microhardness profile for samples steam oxidized at 750 °C. The specimen steam oxidized for 10 hours shows the higher hardness values in the coating region compared to the 100- and 1000-hour conditions. The 10-hour duration might have not been sufficient to remove all the defects existing in the 80Ni-20Cr coating on the modified 9Cr-1Mo steel substrate. In the substrate region, both the 10- and 100-hour specimens showed only a little increase in the hardness near the interface, whereas the specimen steam oxidized for 1000 hours showed a higher value at this region.

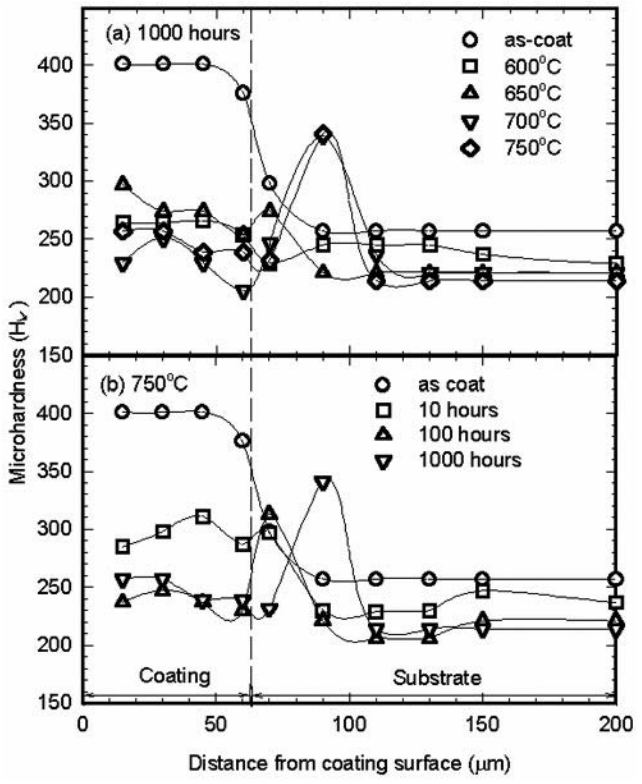

Fig. 7—Microhardness studies of the steam-oxidized specimens for different (*a*) temperatures and (*b*) durations.

D. *Microstructural Characterization*

The SEM investigation was carried out on the etched cross section of the specimens to investigate the microstructure of the hardened layer. Figure 8(a) shows the SEM cross section micrograph for the as-coated specimen. The micrograph clearly distinguishes the 80Ni-20Cr coating and the steel substrate. The coating shows a smooth surface, while the substrate shows a typical tempered martensite structure. The magnified view of the substrate is presented in Figure 8(b). The grains show lath-like structures with a number of white particles. These particles were identified as $M_{23}C_6$ carbides. The lath structure was obtained from the high amount of dislocations produced by the martensite transformation during cooling.[2]

Figure 9 shows the SEM micrographs of the cross-sectional view of the steam-oxidized specimens. The specimen steam oxidized at 600 °C/1000 hours shows a tempered

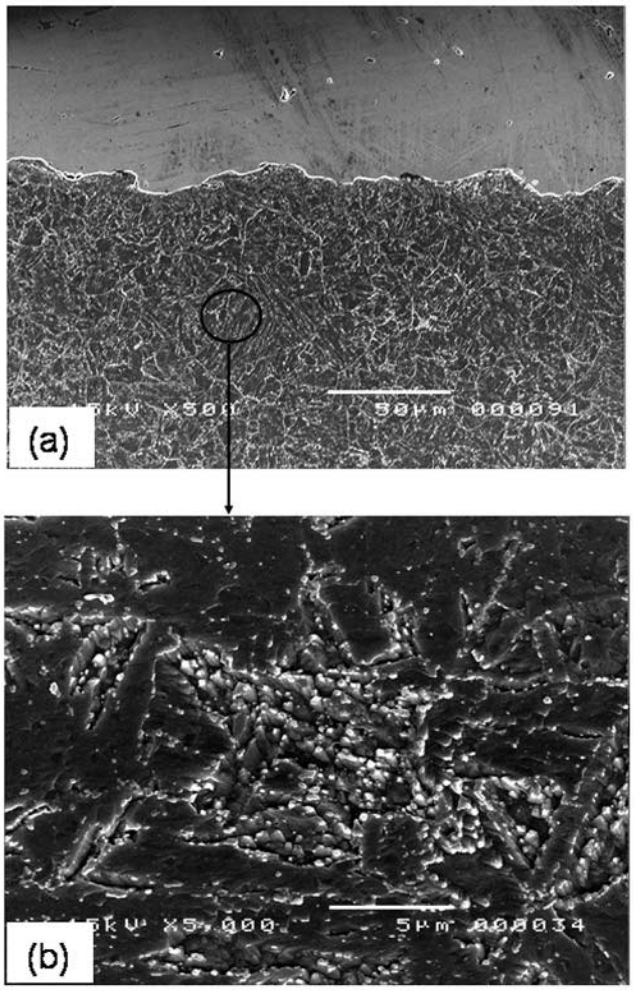

Fig. 8—SEM micrographs of the 80Ni-20Cr-coated modified 9Cr-1Mo steel substrate. The higher magnification of the substrate shows the tempered martensite structure.

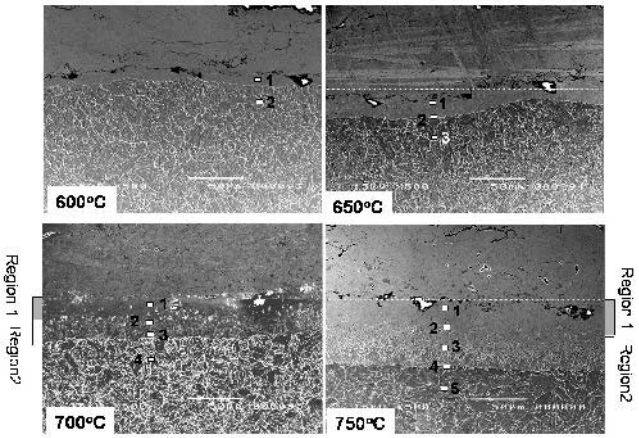

(*a*)

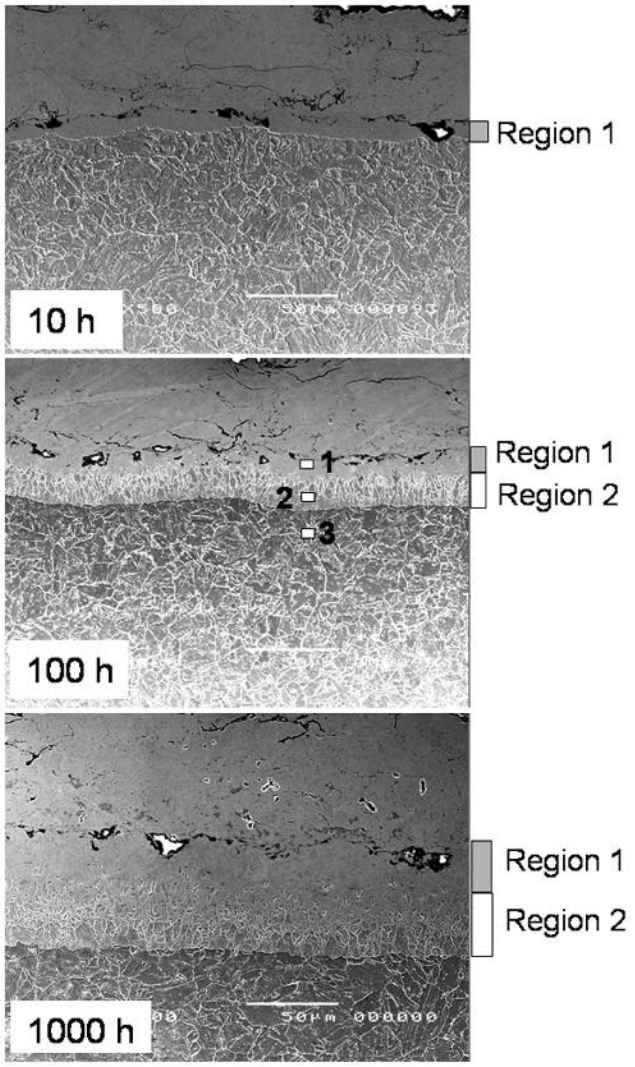

(*b*)

Fig. 9—(*a*) SEM micrographs of the etched substrate after steam oxidation for 1000 h at four different temperatures. The dotted white line approximately indicates the interface between the coating and the substrate. (*b*) SEM micrographs of the etched substrate after steam oxidation at 750 °C for different durations.

martensite microstructure similar to that of the as-coated specimen, except for the region adjacent to the coating, which shows a smooth surface for around 10 μm. This region does not show any clear microstructure even after the etching in vilellas reagent for more than 60 seconds (the recommended etching time is 20 seconds). This reveals that the region is transformed from the tempered martensite to a nonferrite microstructure. Hereafter, for the sake of discussion, this smooth-surface portion is referred as region 1. Increasing the temperature from 600 °C to 650 °C for the same tested duration (1000 hours), the width of the smooth surface increased to around 20 μm. The specimens oxidized at 700 °C and 750 °C showed a further increase in the newly formed region to around 45 and 60 μm, respectively. Within the newly formed regions of the specimens steam oxidized at 700 °C and 750 °C, two different layers appeared. The top layer adjacent to the coating contains a smooth surface (region 1), which is similar to the 600 °C and 650 °C test conditions. Beneath the smooth layer, the secondary layer shows a distinct microstructure (region 2), which is entirely different from the tempered martensite microstructure present in the core substrate. The newly formed regions in the steam-oxidized specimens coincided with the extent of Ni diffusion from the coating to the substrate. This suggests that the Ni diffusion caused either the phase transformation or new compound formation in the tempered martensite microstructure. Figure 8(b) shows the SEM cross-sectional micrographs of the specimens steam oxidized at 750 °C for different durations. At the 10 hour test duration, the substrate region shows a smooth surface region of around 15 μm, which coincided very well with the Ni diffusion shown in Figure 4. However, the modified region shows only the smooth surface and does not show any secondary phase. By increasing the test duration from 10 to 100 and 1000 hours, the modified region extended with two different phases.

The magnified views of regions 1 and 2, along with the core substrate (region 3), are depicted in Figure 10. Region 1 does not reveal any clear microstructure even in the magnified image. This infers that the etchant used for the present observation is not effective in revealing the microstructure in this region. The vilellas reagent is known to be an effective etchant for ferritic microstructures and for observing the transformation products in high-carbon steels. The absence of a clear microstructure even after the etching indicated that the original tempered martensite microstructure transformed to some type of nonferritic microstructure. In the case of region 2, the high-magnification micrograph shows a distinct microstructure, which is entirely different from both the smooth surface of region 1 and the tempered martensite microstructure from the core substrate. This observation suggests that the diffusion of Ni has induced the two different phases transformed from the 9Cr-1Mo steel substrate.

E. *Micro XRD Studies*

Micro XRD studies were employed to identify the phase changes that occurred in the modified 9Cr-1Mo steel substrate due to steam oxidation. The diffraction patterns were obtained from the different microstructural regions indicated in Figure 10.

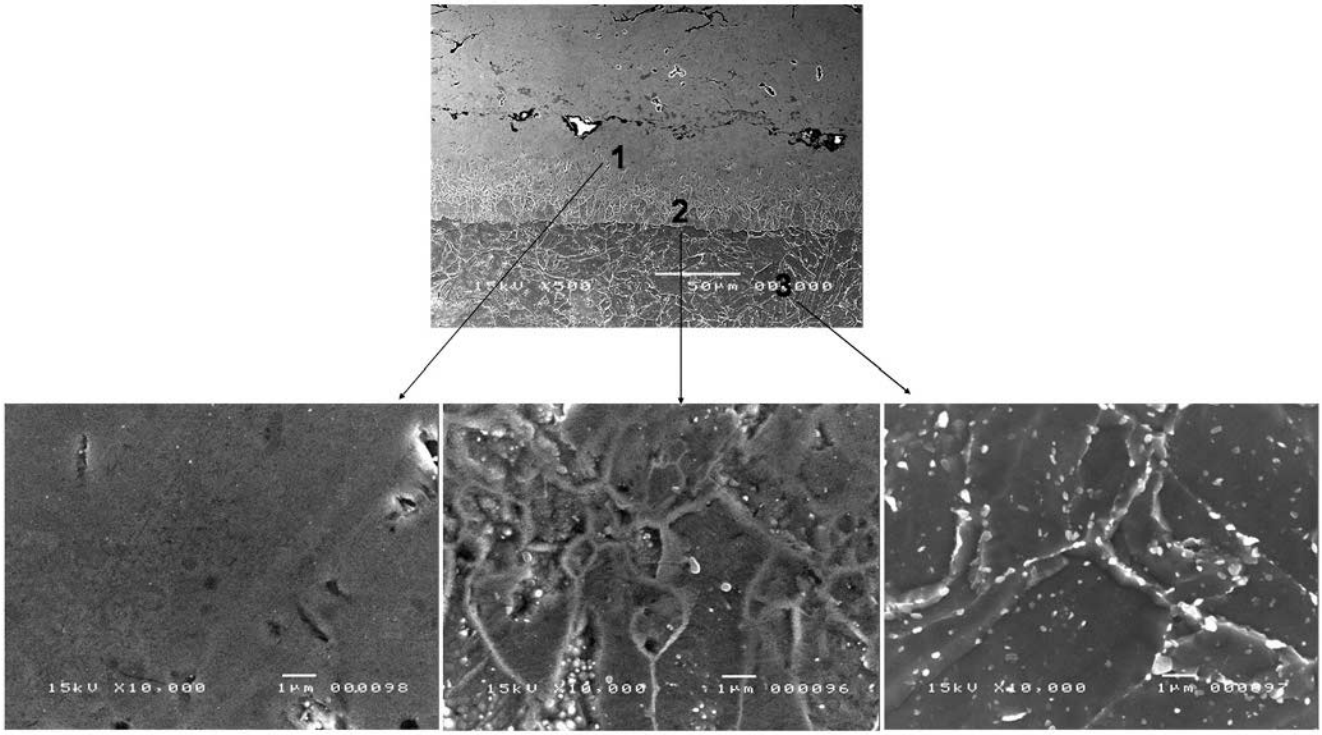

Fig. 10—High-magnification SEM micrographs of different phases obtained from the steam-oxidized specimen after 750 °C for 1000 h.

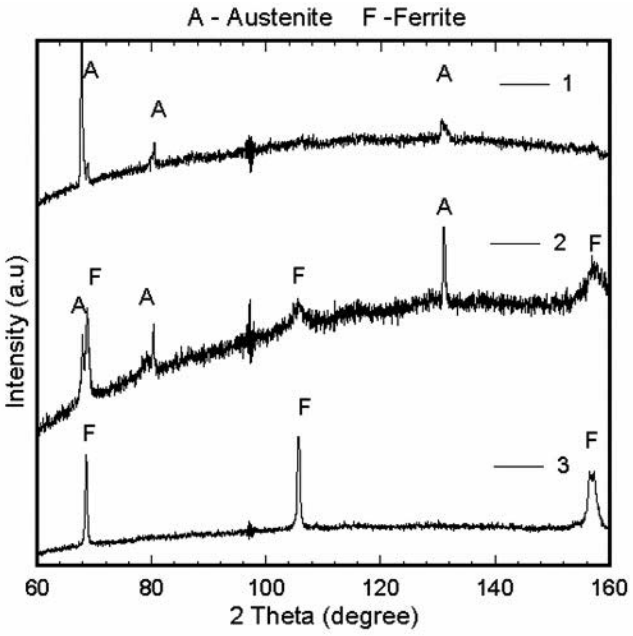

Fig. 11—Micro XRD studies carried out on the three different locations marked in Fig. 9.

Figure 11 shows the XRD patterns for different locations on the modified 9Cr-1Mo steel steam oxidized at 750 °C for 1000 hours. The XRD pattern for the core substrate shows a single ferrite (bcc) phase, as expected. The XRD from region 1 reveals mainly the austenite phase (fcc) and does not show any peak for the ferrite phase. Hence, it is clear that Ni diffusion from the coating to the steel substrate induced the phase transformation from the ferrite to the austenite. On the other hand, the XRD pattern for region 2 consists of two phases: ferrite and austenite. The peaks corresponding to ferrite show peak broadening. This might have arisen from the formation of a martensite phase with a different lattice parameter but with a similar crystal structure. The higher hardness values observed in the specific region of the steam-oxidized specimen arose from the formation of this martensite phase.

By comparing the microhardness distribution in Figure 7 with the cross sections in Figure 9, it is evident that the region with the high hardness corresponds to region 2. More specifically, the specimens steam oxidized at 600 °C/1000 hours and 750 °C/10 hours do not show either a high-hardness region or the secondary phase, whereas all the other specimens show both features.

F. *The EDS Point Analysis*

The points chosen for the EDS analysis are marked in Figure 8. The number of analyzed points was varied for the specimen conditions, depending on the extent of Ni diffusion and, hence, the phase transformation. In the case of specimens steam oxidized at 600 °C for 1000 hours, two points were chosen for the EDS analysis, whereas for the 750 °C/1000 hour condition, five points were taken for the analysis. The mass percentage of Ni and Cr obtained from each point was converted in to the Cr and Ni equivalent with the following equation:

$$\text{Ni equivalent} = (\text{Ni} + (30 \times \text{C})) + (0.5 \times \text{Mn}) \quad [2]$$

$$\text{Cr equivalent} = (\text{Cr} + \text{Mo} + (1.5 \times \text{Si}) + (0.5 \times \text{Nb})) \quad [3]$$

Table III. Summary of the EDS Point Analysis and the Calculated Phase

Number	Specimen °C/h	Position	Mass Pct		Equivalent		Phase
			Cr	Ni	Cr	Ni	
1	base	1	8.7	0	10.0	3.2	M + F
2	600/1000	1	13.4	0	12.4	3.2	A
3		2	11.1	14.6	14.7	17.8	M + F
4	650/1000	1	12.2	30.3	13.5	33.5	A
5		2	11.3	12.4	12.6	15.7	A + M + F
6		3	10.4	0	12.4	3.2	M + F
7	700/1000	1	12.7	23.4	14.1	26.7	A
8		2	10.2	7	11.5	10.2	M
9		3	10.3	5.6	11.5	8.8	M
10		4	10.2	0	11.5	3.2	M + F
11	750/1000	1	10.5	43.2	11.9	49.4	A
12		2	10.5	24.5	11.8	27.8	A
13		3	10.3	15.3	11.7	18.6	A
14		4	10.2	0	11.6	3.2	M + F
15		5	10	0	11.4	3.2	M + F
16	750/100	1	11.3	35.7	12.7	39.1	A
17		2	10.1	2.5	11.4	6.8	M
18		3	10.4	0	11.8	3.2	M + F

A = austenite, M = martensite; and F = ferrite.

The mass percentages of other elements such as C, Mn, Mo, Si, and Nb were assumed to be constant and were taken from Table I. The Ni and Cr mass percentages were obtained from the EDS analysis. It is evident that the Cr equivalent remains in a narrow range of 10 to 14 pct, whereas the Ni equivalent varied from more than 30 pct to 3 pct. The summary of the EDS point analysis (Cr and Ni concentration) on each steam-oxidized specimen, and their respective Cr and Ni equivalents and the possible phase, are given in Table III. The base-steel substrate without steam oxidation exists in the ferrite + martensite phase. For the specimens steam oxidized at 600 °C for 1000 hours, two points were chosen for EDS point analysis, *viz.*, one at the Ni-diffused zone and another at the core substrate. The Ni-diffused area has the Ni equivalent of 17.8 and Cr equivalent of 14.7, which falls in the single austenite phase. On the other hand at point 2, the core substrate microstructure is in the ferrite and martensite phase, the same as the specimen without steam oxidation. From the results, it can be inferred that the temperature at which steam oxidation was carried out did not alter the core substrate microstructure, provided there was no diffusion. In the case of the specimen steam oxidized for 650 °C/1000 hours, three points were chosen among the two points that were located in the Ni-diffused region and the remaining point was at the core substrate. At point 1, located near the coating/substrate interface, the higher Ni content and the Ni and Cr equivalents represent the austenite phase. Point 2 corresponds the mixture of austenite, martensite, and ferrite phases. Point 3, at the core substrate, lies in the martensite and ferrite structure. The specimen steam oxidized at 700 °C for 1000 hours shows the austenite near the interface and, beneath that, the single martensite phase was observed. This indicates that the distinct microstructure observed at region 2 arises from the martensite formation. In the case of 750 °C/1000 hours, a total of five points were chosen, with four points located at the Ni-diffused region and the remaining point at the core substrate. The first three points possess a high amount of Ni and fall into the austenite region. On the other hand, the fourth point shows a very low Ni content and the Ni and Cr equivalent for the point corresponding to the ferrite + martensite phase. From the four points tested in the Ni-diffused region, not even a single point lies on the martensite phase, although the specimen showed higher hardness values and a distinct microstructure in region 2. The diffused Ni formed a concentration gradient in the steel. Points 3 and 4 in the specimens were very near the martensite-forming zone, as shown in Figure 11. The Ni content between these points would fall into the martensite region. If the EDS analysis were carried out between points 3 and 4, it is very likely that the point would fall into the martensite region. The 750 °C/100 hour specimen evinced a point (point 2) whose composition falls in the martensite formation. The overall results suggest that the Ni diffusion induced the observed changes in the phase of the tempered martensite structure. The higher Ni content led to the austenite formation, whereas the lower Ni content transformed into a high-hardness martensite structure.

IV. DISCUSSION

The phase diagram for the modified 9Cr-1Mo steel was calculated with the addition of Ni using the Thermo-Calc software, as shown in Figure 12. The ferrite (α) phase is stable only in a small portion in the diagram. For example, at 750 °C, the ferrite phase is stable while the Ni content is below 1.2 wt pct. When the Ni content goes above 1.2 wt pct, the steel transforms to a dual phase of austenite (γ) + ferrite (α). Above 3.6 wt pct, it remains in the single austenite phase (γ).

On cooling, the transformation from austenite to the original ferrite phase will be limited; if the Ni concentration is increased from an initial content less than 4 mass pct, the substrate will have the potential for transforming to the original ferrite phase. If the Ni content exceeds this limit, it will retain the austenite phase. It is understood

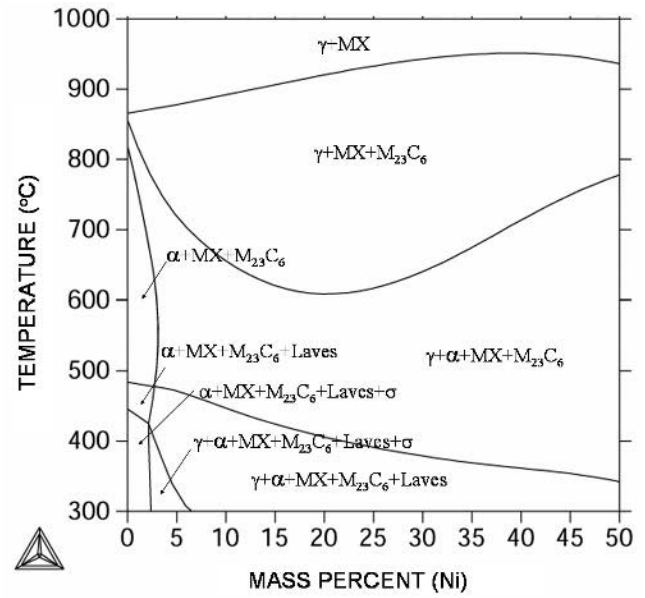

Fig. 12—Calculated phase diagram for the modified 9Cr-1Mo steel with variations in the Ni content.

that the martensite formation occurs during the rapid cooling of the high-temperature austenite. In the case of the present steel, the martensite formation (M_s) starts around 400 °C with even the slow cooing rate adopted.[21] It was reported that the addition of Ni into the steel drastically reduces the M_s temperature. The Ni concentration of 25 wt pct reduced the M_s temperature from 410 °C to 100 °C, and it further decreased with an increase in the Ni content.[22] If the M_s temperature goes below room temperature, the martensite transformation will not occur and the system will retain its austenite phase. In the present system of the Ni-diffused region, there existed a Ni concentration gradient approximately starting from 45 wt pct to 0.04 wt pct (present in the substrate—Table I). The higher-Ni zone will remain in the austenite phase, since the M_s temperature is below room temperature. However, the lower-Ni-concentration zone will transform to the martensite phase due to the higher M_s temperature, which should be above room temperature. This clearly explains the formation of the two-layer austenite + martensite phase in the Ni-diffused zone of the modified 9Cr-1Mo steel.

From the results, the schematic diagrams for the as-coated and steam-oxidized samples are given in Figure 13. In the as-coated condition, the 80Ni-20Cr coating is present on the modified 9Cr-1Mo steel substrate without any interdiffusion. On steam oxidation, the coating and the substrate adjacent to the coating undergo significant changes that include Cr enrichment at the surface to form Cr-rich oxide. The formation of Cr-rich oxide at the surface acts as the barrier for further scale growth and protects the substrate against the steam oxidation. At the interface, a small amount of chromium carbides are formed as islands. Diffusion of Fe from the substrate to the coating occurs, and the magnitude of diffusion is increased with an increase in the temperature and the duration. Similarly, Ni diffuses from the coating to the substrate. The distance of the Ni and Fe diffusion are almost the same, but in the opposite directions of the concentration gradients. The Ni diffusion to the substrate induces the changes in the

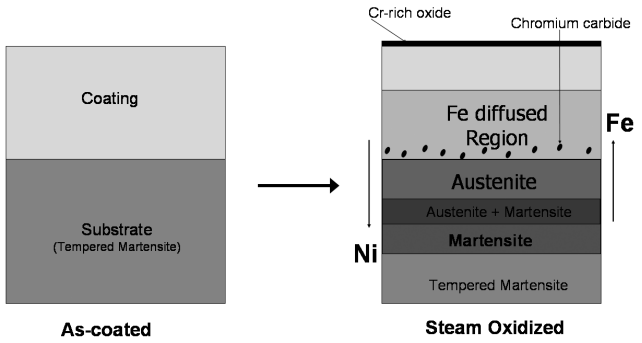

Fig. 13—Schematic representation of the change in structure and morphology due to steam oxidation for 80Ni-20Cr-coated modified 9Cr-1Mo steel.

phase and microstructure. The region adjacent to the coating/substrate interface contains a high Ni content and, thus, transforms into austenite phase during the oxidation test. During the cooling after the oxidation test, the higher-Ni-content zone retains its austenite phase, whereas the lower-Ni-content region transforms to the high-hardness martensite phase.

V. CONCLUSIONS

The 80Ni-20Cr coatings on a 9Cr-1Mo steel substrate showed an excellent steam-oxidation resistance. During steam oxidation, the diffusion of Ni from the coating to the substrate was found to occur, and it influenced the change in microstructure and the hardness. An attempt was made to understand the change of microstructure of the Ni-diffused layer. The results showed that the Ni diffusion caused the original tempered martensite microstructure of the steel substrate to transform into the austenite and martensite microstructures. The rate of Ni diffusion was found to follow the parabolic law, and the extent of the Ni-diffused zone at 750 °C for 1000 hours was 56 μm.

ACKNOWLEDGMENTS

The authors are thankful to Messrs. T. Awane and K. Nishida for their technical help in the EDS and EPMA analysis. The first author (TS) thanks Drs. S.K. Albert and K. Laha, IGCAR (India), for their fruitful discussions during their stay at NIMS.

REFERENCES

1. R. Viswanathan and W.J. Bekker: *Mater. Eng. Performance*, 2001, vol. 10, p. 81.
2. M. Taneike, F. Abe, and K. Sawada: *Nature*, 2003, vol. 424, p. 294.
3. F. Abe, H. Okada, S. Wanikawa, M. Tabuchi, T. Itagaki, K. Kimura, and K. Yamaguchi: *1st Int. Conf. on Advances in Structural Steels*, Tsukuba, Japan, May 22–24, 2002.
4. F. Abe: *Metall. Mater. Trans. A*, 2003, vol. 34A, p. 913.
5. H. Kutsumi, S. Muneki, T Itagaki, and F. Abe: *J. Jpn. Inst. Met*., 2002, vol. 66, p. 997.
6. W. Kaysser: *Surf. Eng*., 2001, vol. 17, p. 305.
7. C. Cheng, G.H. Meier, R.A. Perkins, and W.T. Bekker: in *Materials for Coal Gasification*, W.T. Bekker, ed., ASM INTERNATIONAL, Metals Park, OH, 1988, p. 159.
8. R. Burgel and I. Kvernes: *High-Temperature Alloys for Gas Turbine and Other Applications*, Conf. Proc., W. Betz, ed., Dordrecht, Germany, 1986, p. 327.
9. T. Sundararajan, S. Kuroda, T. Itagaki, and F. Abe: *Iron Steel Inst. Jpn. Int*., 2003, vol. 43, p. 95.

10. T. Sundararajan, S. Kuroda, T. Itagaki, and F. Abe: *Iron Steel Inst. Jpn. Int*., 2003, vol. 43, p. 104.
11. T. Sundararajan, S. Kuroda, K. Nishida, T. Itagaki, and F. Abe: *Iron Steel Inst. Jpn. Int*., 2004, vol. 44, p. 139.
12. T. Sundararajan, S. Kuroda, T. Itagaki, and F. Abe: in *Thermal Spray 2003: Advancing the Science & Applying the Technology*, C. Moreau and B. Marple, eds., ASM INTERNATIONAL, Materials Park, OH, 2003, p. 495.
13. T. Sundararajan, S. Kuroda, and F. Abe: *Mater. Trans*., 2004, vol. 45, p. 1299.
14. T. Sundararajan, S. Kuroda, and F. Abe: *Metall. Mater. Trans. A*, 2004, vol. 35A, p. 3187.
15. T. Sundararajan, S. Kuroda, F. Abe, and S. Sodeoka: *Surface Coating Technol*., in press.
16. M.H. Li, Z.Y. Zhang, X.F. Sun, J.G. Li, F.S. Yin, W.Y. Hu, H.R. Guan, and Z.Q. Hu: *Surface Coating Technol*., 2003, vol. 165, p. 241.
17. *NRIM Creep Data Sheet 2003*, National Institute for Materials Science, Japan, vol. 43, p. 1.
18. J. Porcayo-Calderon, E. Brito-Figueroa, and J.G. Gonzalez-Rodriguez: *Mater. Lett*., 1999, vol. 38, p. 45.
19. E.A. Brandes and G.B. Brook: *Smithells Metals Handbook*, Butterworths–Heinemann, 1992, pp. 131-311.
20. J.C. Lippold: *ASM Handbook*, ASM INTERNATIONAL, Materials Park, OH, 1993, vol. 6, p. 431.
21. U. Boese, D. Werner, and H. Wirtz: *Behavior of Steels during Welding*, Verlag DVS, Dusseldorf, 1984, p. 265.
22. L. Beres: *Welding J*., 1998, vol. 77, p. 273s.